文章编号 1004-924X(2011)02-0200-13

利用激光实时频谱直接观测分子结构变化

TAKAYOSHI KOBAYASHI[1,2,3,4]

(1. University of Electro-Communications, 1-5-1 Chofugaoka, Chofu, Tokyo 182-8585, Japan; 2. ICORP, JST, 4-1-8 Honcho, Kawaguchi, Saitama, 332-0012, Japan; 3. Department of Electrophysics, National Chiao-Tung University, Hsinchu 30010, China; 4. Institute of Laser Engineering, Osaka University, 2-6 Yamada-oka, Suita, Osaka 565-0971, Japan)

摘要:利用脉宽小于 5 fs 的激光脉冲超快光谱同时研究了 Ru$^{\text{II}}$(TPP)(CO)的电子弛豫和振动动力学。研究认为,由$^1Q_{x(1,0)}(\pi,\pi^*)$ and $^1Q_{x(0,0)}(\pi,\pi^*)$产生的信号按$^1Q_{x(1,0)}(\pi,\pi^*)\rightarrow{}^1Q_{x(0,0)}(\pi,\pi^*)\rightarrow{}^3(d,\pi^*)\rightarrow{}^3(\pi,\pi^*)$ 和$^1Q_{x(0,0)}(\pi,\pi^*)\rightarrow{}^3(d,\pi^*)\rightarrow{}^3(\pi,\pi^*)$的顺序从高能态衰减到低能态。$^1Q_{x(1,0)}(\pi,\pi^*)$,$^1Q_{x(0,0)}(\pi,\pi^*)$,$^3(d,\pi*)$,和$^3(\pi,\pi*)$的电子寿命依次为(230±70) fs,(1 150±260) fs,(2 150±360) fs 和极大于 4.8 ps。$^3(d,\pi^*)$和$^3(\pi,\pi^*)$的寿命估计为(2150±360) fs 和极大于 4.8 ps。计算动态 Stokes-shift 过程中的能量衰减率,得到了从$^1Q_{x(1,0)}(\pi,\pi^*)$到$^1Q_{x(0,0)}(\pi,\pi^*)$的渡越时间为(190 ± 40) fs,表明$^1Q_{x(1,0)}(\pi,\pi^*)$的寿命与该渡越时间有相对较好的一致性。对频谱图的分析表明,依赖时间变化的振动光谱与自旋态变化有关,自旋态可以通过曲线交叉点或者单态和三重态之间的势能面的圆锥交面从激发单重态中的 Franck -Condon 态变化到三重态。研究发现,不能简单地使用单重态信号频谱的指数衰减形式和三重态振动信号频谱的指数增长形式来表示这种动态变化。相反,振动频谱的变化伴随着复杂的动态变化。首先,单重态振动频谱发生衰减,然后产生不同于单重态和三重态的新的振动频谱。新的振动频谱增长和衰减后,三重态的振动频谱开始增长。这种动态变化似乎与电子频谱的动态变化不同,将这种明显差异的原因解释为:振动频谱的变化可以敏感地检测处于平衡点和过渡状态或者接近锥形交集状态中的单重态和三重态的结构差异。

关 键 词:振动光谱;超快光谱学;激光光谱法;分子结构;自旋;动力学

中图分类号:O657.319 **文献标识码**:A **doi**:10.3788/OPE.20111902.0200

Direct observation of molecular structural change during intersystem crossing by real-time spectroscopy with a few optical cycle lasers

TAKAYOSHI KOBAYASHI[1,2,3,4]

(1. *University of Electro-Communications*, 1-5-1 *Chofugaoka*, *Chofu*, *Tokyo* 182-8585, *Japan*; 2. *ICORP*, *JST*, 4-1-8 *Honcho*, *Kawaguchi*, *Saitama*, 332-0012, *Japan*; 3. *Department of Electrophysics*, *National Chiao-Tung University*, *Hsinchu* 30010, *China*; 4. *Institute of Laser Engineering*, *Osaka University*, 2-6 *Yamada-oka*, *Suita*, *Osaka* 565-0971, *Japan*)

Abstract: The ultrafast spectroscopy by a sub 5 fs pulse laser was applied to the simultaneous study of electronic relaxation and vibrational dynamics in Ru$^{\text{II}}$(TPP)(CO). The signals due to $^1Q_{x(1,0)}(\pi,\pi^*)$ and $^1Q_{x(0,0)}(\pi,\pi^*)$ are thought to decay in a sequential order from the higher energy states to the low-

收稿日期:2010-10-08;**修订日期**:2010-10-30.

基金项目:Supported by Foundation of Ministry of Education of Chinese Taiwan

er energy states in the sequences $^1Q_{x(1,0)}(\pi,\pi^*)\rightarrow{}^1Q_{x(0,0)}(\pi,\pi^*)\rightarrow{}^3(d,\pi^*)\rightarrow{}^3(\pi,\pi^*)$ and $^1Q_{x(0,0)}(\pi,\pi^*)\rightarrow 3(d,\pi^*)\rightarrow{}^3(\pi,\pi^*)$. The electronic lifetimes of $^1Q_{x(1,0)}(\pi,\pi^*)$, $^1Q_{x(0,0)}(\pi,\pi^*)$, $^3(d,\pi^*)$, and $^3(\pi,\pi^*)$ are determined to be (230±70) fs, (1150±260) fs, (2150±360) fs and larger than 4.8 ps, respectively. The lifetimes of $^3(d,\pi^*)$, and $^3(\pi,\pi^*)$ are estimated to be (2 150 ± 360) fs and larger than 4.8 ps, respectively. The lifetime of $^1Q_{x(1,0)}(\pi,\pi^*)$ determined to be (230 ± 70) fs, is in relatively good agreement with the step-down time of (190±40) fs for the transition time from $^1Q_{x(1,0)}(\pi,\pi^*)$ to $^1Q_{x(0,0)}(\pi,\pi^*)$ calculated from the energy decay rate in the dynamic Stokes-shift process. The spectrogram analysis shows that the time dependent changes in the vibrational spectrum is associated with the spin state change from the Franck-Condon state in the excited singlet state to the triplet state via the curve crossing point or conical intersection between the singlet and triplet potential surfaces. It is found that the dynamics is can not be expressed in terms of the simple single exponential decay of the spectrogram signal of singlet and exponential growth of the triplet vibration spectrogram signal. In stead, the vibrational spectral change takes place with more complex dynamics. At first, the decay of the singlet vibration spectrum takes place and then new vibrational spectrum which is different from singlet and triplet states appears. After the growth and decay of the new vibrational spectrum, the triplet state vibration spectrum starts to grow. The dynamics at first looks different from that of electronic spectra. The reason of the apparent difference can be explained in the following way. The vibrational spectral change could sensitively detect the structural difference among the singlet sate and triplet state in their equilibriums and that of transition state or state close to the conical intersection.

Key words: vibration spectrum; ultrafast spectroscopy; laser spectroscopy; molecular structure; spin; dynamics

1 Introduction

Metallo-porphyrin complexes have been extensively studied as model complexes for many important biological systems. The report of the oxidation reaction of Ru^{II}(TPP)(CO) [TPP = tetraphenylporphyrin] in 1973[1] triggered numerous studies of Ru^{II}(TPP)(CO) as a model complex of Fe^{II}(por) [por = porphyrin], and a central skeleton of hemoglobin which functions as an oxygen transport in human bodies. However, detailed studies have not yet been conducted on the excited state dynamics of Ru^{II}(TPP)(CO). It is known that the lowest excited triplet state in Ru^{II}(CO) porphyrin was $^3(\pi,\pi^*)$[2], and the phosphorescence lifetime in Ru^{II}(TPP)(CO)(py) [py = pyridine] was measured to be 35 μs at room temperature[3a]. The fluorescence lifetime has not been yet resolved but it was reported to be shorter than 30 ps in 1999[3a] and 1 ps in 2005[3b]. Additionally, it is desired to elucidate the mechanism of intersystem crossing in the metal-porphyrin complex reaction[4]. In general, the information obtained from signals due to pure electronic dynamics was not enough to elucidate the relaxation process of the electronic excited states[5]. The real-time vibrational spectroscopy provides the modulated probability of electronic transition by molecular vibration. By this method, we can obtain both the information of the radiation-less electronic relaxation and that of the instantaneous vibrational frequency during the relaxation at the same time using a single experimental system, satisfying completely same experimental conditions.

2 Experimental section

2.1 Broadband visible pulse generation by NOPA

By using a Non-collinear Optical Parametric Amplifier (NOPA) shown in Fig. 1, we obtained an ultra-broadband visible pulse, which can be compressed to sub-5 fs for the ultrafast pump-probe measurement.

As a laser source, a Ti:sapphire regenerative amplifier (Spectra-Physics, model Spitfire, 150 μJ, 100 fs, 5 kHz at 805 nm) was used to generate pump and seed pulses of the NOPA. A single-filament white light continuum was generated in a sapphire plate with a thickness of 1 mm as the seed pulse. The seed pulse was non-collinearly amplified in a NOPA crystal (type I-BBO, $\theta=31.5°$) pumped by a second harmonics (SH, 100 μJ) of the laser source. The SH used for the pump pulse of NOPA was generated by a BBO crystal with a thickness of 0.4 mm to obtain the broadband SH pulse.

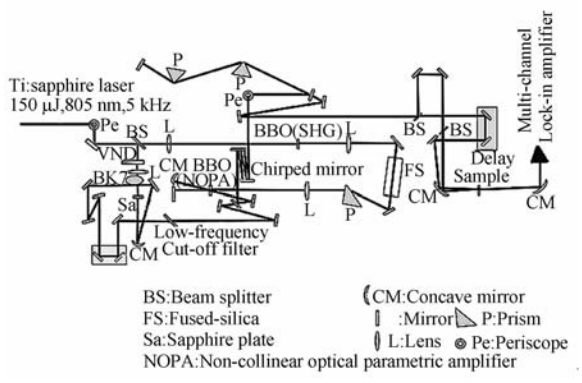

Fig. 1 NOPA for sub 5 fs pump-probe measurement system

After amplification by the NOPA, a main compressor compensates the residual chirp. The total pulse compressor is composed of the Ultra-Broadband Chirped Mirror (UBCM, Hamamatsu Photonics) pair, a 45° fused-silica prism pair, and Cr-coated broadband beam-splitters with the thickness of 0.5 mm. The UBCM pair with three round trips and prism pair are for the main compression. The amplified signal pulse after the double-pass NOPA with a spectrum extending from 525 to 725 nm was compressed with the main compressor resulting in a pulse duration of sub 5 fs which is nearly Fourier transform limited.

2.2 Pump-probe measurement

We used a sub 5 fs pulse to observe the real-time vibrational dynamics associated with the relaxation in the electronic states of Ru^{II}(TPP)(CO) in $CHCl_3$, a non-coordinating solvent[7]. The spectra of the sub 5 fs pulses covered from 525 to 725 nm with a nearly constant phase (Fig. 2). The polarizations of the pump and the probe beams were parallel to each other. The intensities of the pump and probe pulses were (2 880±300) and (480±50) GW·cm^{-2}, respectively. The focus areas of the pump and probe pulses were 100 μm^2 and 75 μm^2, respectively.

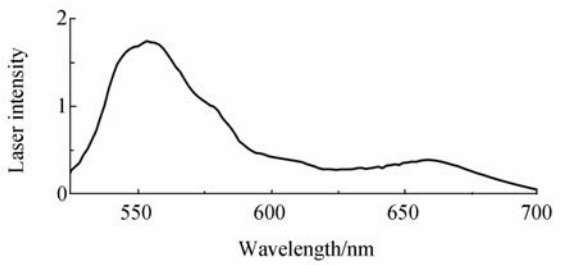

Fig. 2 Laser spectrum of sub 5 fs pulses used for pump pulse and probe pulse from 525 to 725 nm

All measurements were performed at (295±1) K using the sample solution in a 1 mm cell. Time-resolved difference transmittance ΔT in the spectral range from 525 to 700 nm was measured simultaneously using a multi-channel lock-in amplifier coupled to a polychromator (300 grooves/mm, 500 nm blazed) and avalanche photodiodes through a 128 channel fiber bundle. The spectral resolution of the system was about 1.57 nm. The transmitted probe spectrum after the sample without the injection of the pump was recorded by averaging 50 000 laser shots. The transmission difference of the probe was ac-

cumulated every 3 000 laser shots under the excitation conditions by the pump pulse. The pump-probe experiment was performed with a 1 fs step from 100 to 4 800 fs.

2.3 Group Velocity Dispersion (GVD)

Refractive index of chloroform is $n = 1.431\,364 + 5\,632.41/\lambda^2 - 2.080\,5 \times 10^8/\lambda^4 + 1.261\,3 \times 10^{13}/\lambda^6$[8]. Therefore GVD of chloroform is calculated as Fig. 3. The pulse width after transmission through a 1 mm cell was calculated to be about 40 fs.

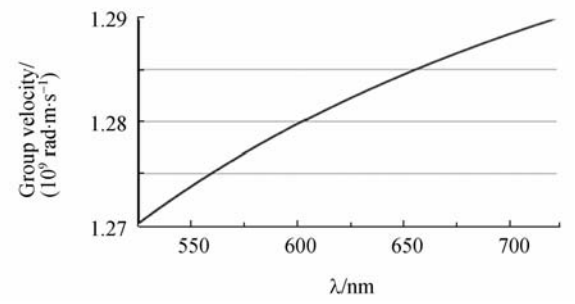

Fig. 3　Group velocity dispersion of chloroform

Since the electronic relaxation time to be discussed in this paper was found to be longer than 200 fs, the effect of GVD on the electronic relaxation dynamics is negligible. On the other hand, the effect in vibrational dynamics can be substantial, because the stretched pulse width attenuates the amplitude of molecular vibration observed in the signal as shown in Fig. 4(a). The amplitudes of vibration modes with frequencies between 800 and 1 200 cm^{-1} discussed in this article are reduced because of their short vibrational period, which cannot be properly resolved by the stretched pulse similar to or longer than the periods. However, the value of vibration frequency is not affected. Hence the frequency and its shift can still be correctly discussed. As is seen in Fig. 4(a), the effect of pulse width is almost the same in the vibration frequencies from 800 to 1 200 cm^{-1}. The amplitude of high frequency modes were corrected using the calculated results shown in Fig. 4(b).

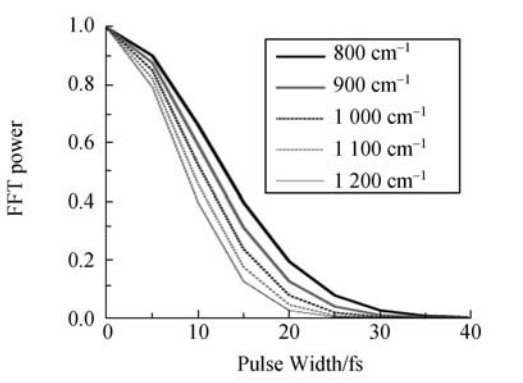

Fig. 4(a)　Simulation result to show the effect of reduction of normalized FFT power of real-time traces with vibration frequencies from 800 to 1 200 cm^{-1} measured with different pulse widths from 0 to 40 fs

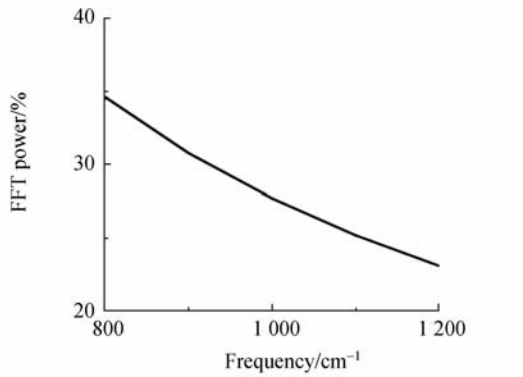

Fig. 4(b)　Simulation result of the loss in observed FFT power of vibration modes from 800 to 1 200 cm^{-1} measured for chloroform in a cell

2.4 Robustness of the sample against laser irradiation

The (d,π^*) excitation induces the π back donation of Ru($d\pi$)→CO(π^*) and photo-dissociates CO with quantum yield of 1.9×10^{-4}[2b,9]. To investigate the effect of photo-dissociation in the procedure of pump-probe experiment, we estimated the rate of photo-dissociation of Ru(por)CO. After being excited by a single laser pulse, 8×10^5 of Ru(por)CO molecules are to be photo-dissociated. Experimental time required for the photo-dissociation of 10% of Ru(por)CO was then calculated to be about 24 s. While the Stokes equation $f = 6\pi a\eta$, where the radius of Ru

porphyrin a and the viscosity of chloroform η are 1.8×10^{-9} m and 0.57×10^{-3} kg·m^{-1}·s^{-1}, respectively, and diffusion coefficient $D=kT/f$ can give the calculated result that the diffusion length of the molecule is about 50 m in 24 s, which induces 125 times dilution of the photo-dissociated molecule. Therefore, the above calculation shows that the effect of the photo-dissociation is negligible.

In addition, we found that the absorption spectrum did not change before and after the experiment even when the amount of the sample is only xx times larger than the irradiation volume.

2.5 Spectroscopy

Ultraviolet/Visible (UV/Vis) spectra were recorded on a Shimadzu model UV-3101PC spectrometer. Emission spectra were recorded on a HITACHI model F-4500 fluorescence spectrophotometer.

3 Results

Real-time traces from 100 to 4 800 fs of the absorbance change (ΔA) and probe wavelength dependency of ΔA (525－700 nm) obtained in the pump-probe measurement are shown in Fig. 5 and Fig. 6, respectively. Fig. 6 shows that the difference absorption spectrum ($\Delta A(\omega)$). The difference absorbance, ΔA, is negative over the entire probe wavelength range in the full delay-time range. The time-resolved spectrum at delay time earlier than 1 ps has a peak wavelength and width similar to the stimulated emission spectrum ($\lambda_{max}=595$ nm) of Ru^{II}(TPP)(CO) calculated from the fluorescence spectrum (Fig. S1 in Supporting Information)[10]. Since phosphorescence spectrum of Ru^{II}(TPP)(CO)(py) is known to be peaked at $\lambda_{max}=726$ nm[3a], the observed emission peak at $\lambda_{max}=595$ nm was assigned not to phosphorescence but to fluorescence[11]. Even after a careful purification process the emission peak intensity is not reduced, the possibility of impurity can be ruled

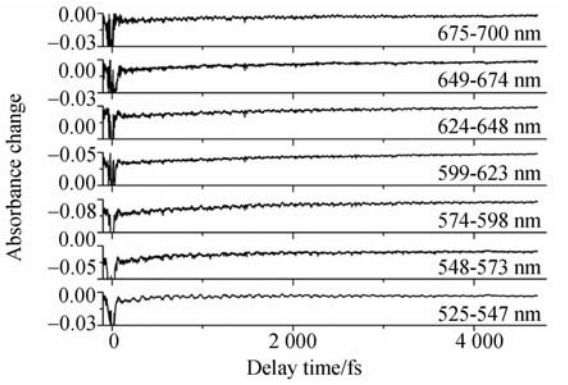

Fig. 5 Real-time traces of induced absorbance changes of Ru^{II}(TPP)(CO) averaged over 16 probe channels in the delay time range between 100 and 4 800 fs

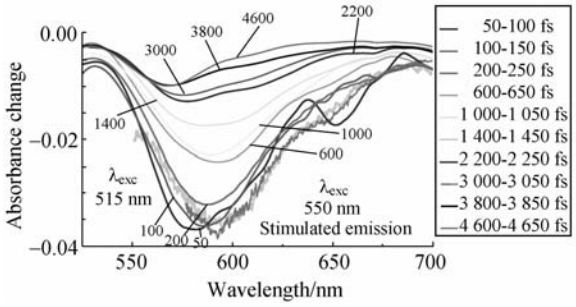

Fig. 6 Difference absorption spectra of Ru^{II}(TPP)(CO) and stimulated emission spectra calculated from fluorescence spectrum[10]. The 10 ΔA spectra at different time regions were obtained by averaging for 50 fs in each time region of 50－100 fs, 100－150 fs, 200－250 fs, 600－650 fs, 1 000－1 050 fs, 1 400－1 450 fs, 2 200－2 250 fs, 3 000－3 050 fs, 3 800－3 850 fs, and 4 600－4 650 fs. Thick curves show stimulated emission spectra, whose excitation wavelengths are 515 nm and 550 nm.

out. The negative peak at 580 nm appears at a delay time shorter than 100 fs, and is red-shifted to 591 nm after 100 fs. This red shift occurs at a rate of (0.67 ± 0.15) eV·ps^{-1} and is considered to be due to a dynamic Stokes-shift. This corresponds to the step down time from higher vibrational levels to the lower level of the mode coupled to the electronic state. The coupled mode frequency can be calculated from energy differ-

ence between $Q_x(1,0)$ (18 939 cm^{-1}) and $Q_x(0,0)$ (17 897 cm^{-1}) as 1 042 cm^{-1}. Therefore, from the red-shift rate of (0.67±0.15) eV·ps^{-1}, the step-down time on the vibrational ladder is determined to be 1 042 cm^{-1}/(0.67±0.15) eV·ps^{-1}=190±40 fs. The ΔA signal is mainly due to the stimulated emission from $^1Q_{x(0,0)}(\pi,\pi^*)$, whose lifetime was determined by the analysis described below.

4 Discussion

Singular-valued decomposition (SVD) analysis of the time-resolved traces provides four decay time constants (τ_1, τ_2, τ_3, and τ_4) as shown in Fig. 7. Using the average of lifetimes obtained at 128 probe wavelength channels, τ_1, τ_2, τ_3, and τ_4 were determined to be (230±70) fs, (1 150±260) fs, (2 150±360) fs, and 4.6 ps, respectively. The decay time constants were obtained by fitting the time-resolved ΔA trace recorded up to the delay time of 4.8 ps. Considering limited accuracy of the fitted time constant shorter enough than 4.8 ps, the signal component with the decay time of 4.6 ps was included in the constant component in the analysis. The UV/Vis absorption spectrum of Ru^{II}(TPP)(CO) has a $Q_x(1,0)$ band peak at λ_{max}=528 nm (18 939 cm^{-1}) and a $Q_x(0,0)$ band peak at λ_{max}=560 nm (17 897 cm^{-1}) as shown in Fig. 8. The laser spectrum from 525 to 725 nm covers both of the absorption bands, therefore Ru^{II}(TPP)(CO) was coherently excited into both of the $^1Q_{x(0,0)}(\pi,\pi^*)$ and $^1Q_{x(1,0)}(\pi,\pi^*)$ states. The FFT amplitude of 1 040 cm^{-1}, which is energy difference between $Q_x(1,0)$ and $Q_x(0,0)$ band, was proportional to the pump intensity as shown in Fig. 9. The ratio of the excited population density between $Q_x(0,0)$ and $Q_x(1,0)$ was calculated to be 1.92 : 1 from the absorption and laser spectra. The signals due to $^1Q_{x(1,0)}(\pi,\pi^*)$ and $^1Q_{x(0,0)}(\pi,\pi^*)$ are thought to decay in a sequential order from the higher energy states to the

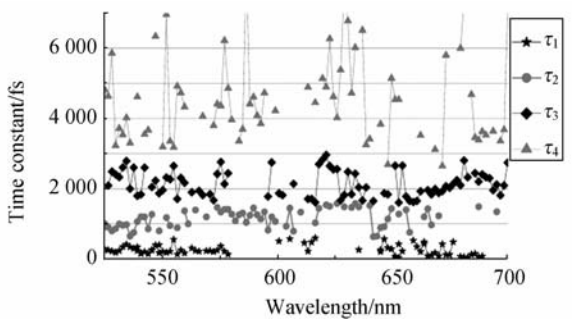

Fig. 7　Probe wavelength dependence of lifetimes of intermediates obtained by singular-value decomposition analysis

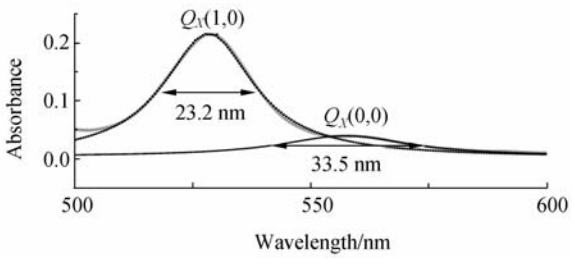

Fig. 8　Visible absorption spectra of $Q_x(1,0)$ and $Q_x(0,0)$ of Ru^{II}(TPP)(CO). They were obtained from the absorption spectrum of sample fitting by two Lorentzian functions ($Q_x(1,0)$: black dots, $Q_x(0,0)$: black line)

lower energy states in the sequences $^1Q_{x(1,0)}(\pi,\pi^*)\rightarrow{}^1Q_{x(0,0)}(\pi,\pi^*)\rightarrow{}^3(d,\pi^*)\rightarrow{}^3(\pi,\pi^*)$ and $^1Q_{x(0,0)}(\pi,\pi^*)\rightarrow{}^3(d,\pi^*)\rightarrow 3(\pi,\pi^*)$. The real-time A traces are expected to be fitted well with the following equation.

$$f(t)=(1.92/2.92)\,[(A_1(\exp(-t/\tau_1))+A_2(\exp(-t/\tau_2)-\exp(-t/\tau_1))+A_3(\exp(-t/\tau_3)-\exp(-t/\tau_2))+A_4(1-\exp(-t/\tau_3))]+(1/2.92)[A_2(\exp(-t/\tau_2)-\exp(-t/\tau_1))+A3(\exp(-t/\tau_3)-\exp(-t/\tau_2))+A_4(1-\exp(-t/\tau_3))]=(1.92/2.92)\,(A_1(\exp(-t/\tau_1))+A_2(\exp(-t/\tau_2)-\exp(-t/\tau_1))+A_3(\exp(-t/\tau_3)-\exp(-t/\tau_2))+A_4(1-\exp(-t/\tau_3)),\quad(1)$$

The spectra of components A_1, A_2, A_3, and A_4 thus obtained are shown in Fig. 10. The signal of A_2, which has a negative peak at λ_{max}=591 nm, is attributed to the stimulated emission from $^1Q_{x(0,0)}(\pi,\pi^*)$, based on its agreement with the stimulated emission spectrum (λ_{max}=

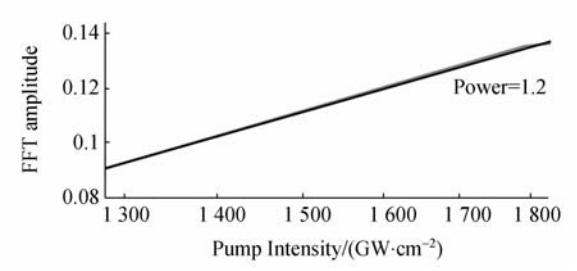

Fig. 9　Pump intensity dependence of vibrational amplitude of porphyrin ring stretching mode

595 nm, Fig. 10) calculated from the fluorescence spectrum (Fig. S1). Therefore, the lifetime of $^1Q_{x(0,0)}(\pi,\pi^*)$ was estimated to be 1 150 fs($=\tau_2$).

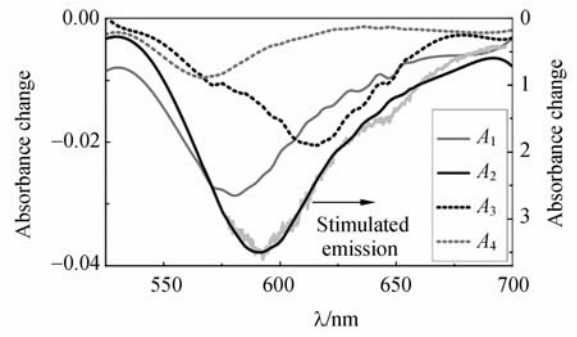

Fig. 10　Spectra of four components obtained by sequential model

Spectrum A_1 has a negative peak at $\lambda_{max}=580$ nm, which is 11 nm longer than that of A_2. Both the negative peaks are reasonably attributed to stimulated emission because of impossible assignment to the bleaching due to the lack of absorption in the spectral range and from the peak wavelength close to that of the spontaneous emission spectrum. Therefore, A_1 can be attributed to the stimulated emission from $^1Q_x(1,0)(\pi,\pi*)$ with a lifetime of 230 fs ($=\tau_1$). The lifetime of the A_1 signal is shorter than that in A_2. The reason why the peak wavelength of stimulated emission band A_1 is shorter than that of A_2, can be explained as follows. The minimum of potential energy surface of excited state is displaced from that of the ground state. Therefore, $Q_x(1,0)$ can have not only the transition of $\nu_1'\rightarrow\nu_1$, but also higher energy transitions ($\nu_1'\rightarrow\nu_0$) and lower energy transitions ($\nu_1'\rightarrow\nu_2$ and $\nu_1'\rightarrow\nu_3$). In the same way, in the case of $Q_x(0,0)$, the transfer can not only be $\nu_0'\rightarrow\nu_0$ but also lower energy transitions like $\nu_0'\rightarrow\nu_1$ and $\nu_0'\rightarrow\nu_2$. The transfer energies of $\nu_0'\rightarrow\nu_0$ and $\nu_1'\rightarrow\nu_1$ are close to each other, because both of $Q_x(1,0)$ and $Q_x(0,0)$ belong to the same electronic state in the lowest vibrational levels expected to have minimal anharmonicity. However, above mentioned higher transition energy of $\nu_1'\rightarrow\nu_0$ compared with that of $\nu_1'\rightarrow\nu_1$ caused the blue shift of A_1, which has a peak at 11 nm shorter than that of A_2. As mentioned above the lifetime of A_1 due to $^1Q_{x(1,0)}(\pi,\pi^*)$ is determined to be (230±70) fs. This result is in relatively good agreement with the step-down time of (190±40) fs for the transition time from $^1Q_{x(1,0)}(\pi,\pi^*)$ to $^1Q_{x(0,0)}(\pi,\pi^*)$ calculated from the energy decay rate in the dynamic Stokes-shift process. Moreover, the hypothesis of the spectral component A_1 being due to the stimulated emission from $^1Q_{x(1,0)}(\pi,\pi^*)$ is supported by the following observed phenomena. The ratio between FWHMs of A_1[related to $Q_x(1,0)$] and A_2[related to $Q_x(0,0)$] was determined to be 58.6 nm/49.6 nm=1.2±0.1(Fig. 10). While, the ratio between FWHMs of $Q_x(1,0)$ and $Q_x(0,0)$ bands in the UV/Vis spectra was 23.2 nm∶33.5 nm=(1∶1.44) ± 0.02(Fig. 8). The observation that A_2 has a broader bandwidth than A_1 is consistent with the $Q_x(1,0)$ band being broader than the $Q_x(0,0)$ band.

The component A_3 with a negative peak at $\lambda_{max}=616$ nm and the longer lifetime than A_2 is concluded to be due to the stimulated emission from the triplet excited state as follows. The intersystem crossing from $^1(\pi,\pi^*)$ to $^3(d,\pi^*)$ is thought to take place more easyly than the spin-forbidden intersystem crossing from $^1(\pi,\pi^*)$ to $^3(\pi,\pi^*)$[9]. Moreover, the charge transfer from the porphyrin ring to the central metal atom enhances the spin-orbit coupling and accelerates intersystem crossing. Therefore, the A_3 spectrum

with a peak at $\lambda_{max}=616$ nm is due to a stimulated emission signal from $^3(d,\pi^*)$. This assignment is also supported by previous reports showing that the phosphorescence from $^3(\pi,\pi^*)$ has a $\lambda_{max}=725$ nm in Ru(tpp)(CO)py[3a] and $^3(d,\pi^*)$ exists close to $^1(\pi,\pi^*)$ between $^1(\pi,\pi^*)$ and $^3(\pi,\pi^*)$[2b]. It is at first sight surprising that the stimulated emission from the triplet state appears to the intensity of about 1/2 of that of the stimulated emission from the singlet state. However, the signal cannot be assigned to the stimulated emission from the singlet state, because the signal appears in the region whose wavelength is longer than that of the spontaneous emission from the singlet state. Therefore, the signal can only be assigned to the stimulated emission from the triplet state. There is no report concerning the S-T absorption of Ru porphyrin complex, whose lowest triplet excited state is (π,π^*), but strong S-T absorption is reported in similar complexes such as Os porphyrin complex and the Ru bipyridine complex which have (d,π^*) as their lowest triplet excited states.[2c,12] It suggests the possibility of stimulated emission from $^3(d,\pi^*)$ of Ru^{II}(TPP)(CO). Moreover, besides strong stimulated emission, there exists the induced absorption from the excited singlet state and the excited triplet state. This can be the reason why the intensity of A_2 is 2 times or more large than that of A_3. Therefore, the lifetime of $^3(d,\pi^*)$ was estimated to be about 2.2 ps ($=\tau_3$).

The component A_4 with a negative peak at $\lambda_{max}=565$ nm, is due to residual (22%) bleaching induced by ground-state depletion remaining even at the longest delay, because Ru^{II}(TPP)(CO) has a $Q_x(0,0)$ absorption band in this spectral range around 565 nm ($\Delta A=0.04$). The phosphorescence from $^3(\pi,\pi^*)$ is reported to have a peak at $\lambda_{max}=725$ nm in Ru(tpp)(CO)Py,[3a] therefore the signal observed around 565 nm after relaxation to $^3(\pi,\pi^*)$ is not due to stimulated emission corresponding to the phosphorescence.

The results of the above analysis and discussion of the electronic state are summarized as follows; the lifetimes of $^1Q_{x(1,0)}(\pi,\pi^*)$, $^1Q_{x(0,0)}(\pi,\pi^*)$, $^3(d,\pi^*)$, and $^3(\pi,\pi^*)$ were determined to be (230±70) fs, (1 150±260) fs, (2 150±360) fs and larger than 4.8 ps, respectively (Fig. 11).

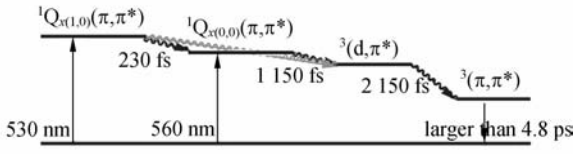

Fig. 11　Energy level diagram and the excited state dynamics including vibrational relaxation from the vibrational level of (1,0) to (0,0), intersystem crossing form $^1Q_x(\pi,\pi^*)$ to $^3(d,\pi^*)$, and internal conversion from $^3(d,\pi^*)$ to $^3(\pi,\pi^*)$.

As a further detailed investigation of the mechanism of the decay dynamics of the intermediate states obtained above, the dynamics of the vibrational state were also analyzed. Using spectrogram analysis, we detected the transitional changes of these molecular vibration modes up to 1 500 fs (Fig. 12). The spectrogram was calculated from the averaged ΔA traces over 10 probe wavelengths around 600 nm using the Blackman window function whose FWHM was 240 fs. The data in the vicinity of 0 fs up to 300 fs could not be measured accurately because of the strong interference between the scattered pump pulse and probe pulse, and hence the results of the spectrogram analysis were shown in the delay time range from 300 to 1 500 fs, where the effect of interference is negligibly small. At 300 fs, the porphyrin ring stretching mode (υ_{por}) was observed around 1 036 cm^{-1}, which agrees well with the calculated frequency (1 040 cm^{-1}) of singlet state Ru^{II}(por)(CO) [Fig. 13(a)][13]. (The calculation method and its detailed results are shown in supporting information.) This frequency is reduced to 1 150 cm^{-1} in several

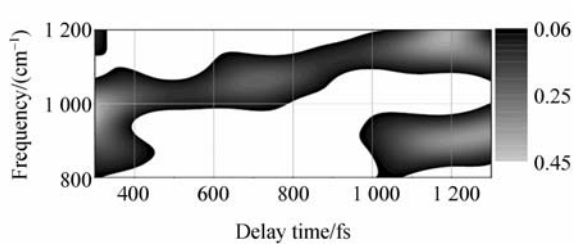

Fig. 12　Fourier power spectrogram calculated from the real-time trace probed around 600 nm. The frequency resolution of the spectrogram was estimated to be 30 cm^{-1} from the gate of FWHM with 240 fs

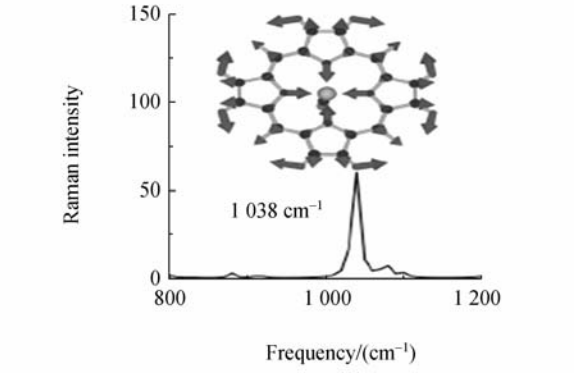

(a) Ground singlet state

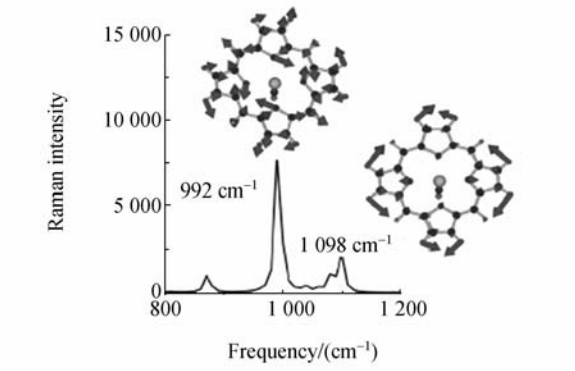

(b) Triplet state

Fig. 13　Calculated Raman spectra

hundreds fs from about 600 fs to 1 ps because of the appearance of the triplet state, whose υ_{por} was obtained by the quantum chemical calculation to be 1 100 cm^{-1}. The peak centered around 900 cm^{-1} that appears at about 1 ps is also considered to be due to the triplet state after the intersystem crossing, because the calculated result suggests the appearance of the porphyrin ring bending mode at 990 cm^{-1}, characteristic of the triplet state in RuII(por)(CO) [Fig. 13(b)].

From the electronic state dynamics analysis as previously described the ultrafast dynamics of Ru^{II}(TPP)(CO) shows that the lifetime of the singlet excited state is about (1.2±0.2) ps, and it is corresponding to the growth of the triplet state. Both positive and negative absorbance changes were assigned to the absorption bands of the transition states.

The electron spin state is thought to change from the singlet into the triplet state with a certain transition probability, therefore we performed a model calculation in which Fourier power of the porphyrin ring stretching mode of 1 040 cm^{-1}(singlet) and that of 1 150 cm^{1}(triplet) decays and grows, respectively, both with a time constant of 1.2 ps. The calculation shows that the two frequency modes keep their original frequencies (Fig. 14). However, experimental results show the presence of intermixing as a gradual blue shift of υ_{por} from 1 040 to 1 150 cm^{-1}. The signal intensity at 1 060 cm^{-1} has a peak at the gate delay time of 640 fs during the course of delay time.

The above-mentioned spectrogram analysis shows that the time dependent changes in the vibrational spectrum associated with the spin state change from the Franck-Condon state in the excited singlet state to the triplet state via the curve crossing point or conical intersection between the singlet and triplet potential surfaces. We calculated the spectrogram of the system in which the singlet state with the vibration mode of 1 040 cm^{-1} decays exponentially with 1.2 ps and triplet state with mode of 1 150 cm^{-1} grows exponentially with the same time constant. The results of spectrogram calculation is shown in Fig. 14. The dynamics was found not be able to be expressed in terms of simple single exponential decay of the spectrogram signal of singlet and exponential growth of the triplet vibration spectrogram signal. Instead, the vibrational

spectral change is taking place with more complex dynamics. At first the decay of the singlet vibration spectrum takes place and then new vibrational spectrum which is different from singlet and triplet state appears. After the growth and decay of the new vibrational spectrum, the triplet state vibration spectrum start to grow. The dynamics at first glance looks different from that of electronic spectra. The reason of the apparent difference can be explained in the following way. The vibrational spectral change could sensitively detect the structural difference among the singlet state and triplet state in their equilibriums and that of transition state or state close to the conical intersection.

This may be due to the bottleneck of wavepacket passage through the curve crossing point between the excited singlet state and excited triplet state. The structural change in Ru^{II} (TPP)(CO) during the transition from the Franck-Condon state to the curve crossing point or conial intersection between the singlet and triplet is followed by the intersystem crossing to the triplet state[14]. The intersystem crossing takes place with a time constant of about 1 ps. This ultrafast intersystem crossing can be due to the heavy atom effect of Ru on the spin-orbit coupling and/or the mediation of high-frequency modes of the molecule in a strong non-Born-Oppenheimer regime[15].

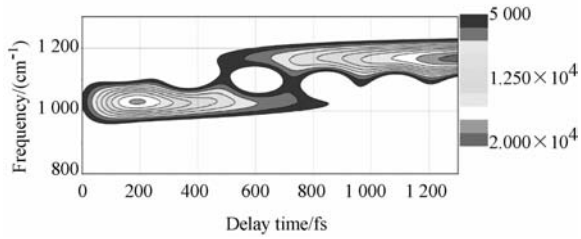

Fig. 14　Simulated data of spectrogram assuming that the modes of 1 040 and 1 150 cm^{-1} decay and rise, respectively, with the same time constant of 1 060 fs

The discussion made above can be rephrased in the following way. When the singlet state is starting relaxation through the intersystem crossing via the mechanism of spin-orbit coupling during the relaxation process, the wavefunction of the state can well be described in terms of the linear combination of the spin singlet and spin triplet. The electronic state of the singlet manifold and triplet manifold are different. However, during the process of the molecular structure is changing gradually and continuously. It means that the Hilbert space of singlet – triplet manifold is only four dimensional but in the electronic structure the Hilbert space is much more complicated namely composed of 3N-6 dimension. The fore even th change is from the singlet state to the triplet state, it is continuously and gradually changing. Especially if it passes through transition state or the conical intersection, it may have some latent stage. This is considered to be the origin of the signal observed in the spectrogram shown in Fig. 14.

In conclusion, both electronic relaxation and vibrational dynamics in Ru^{II} (TPP)(CO) were elucidated simultaneously under the same experimental conditions using a sub 5 fs pulse. From the observed electronic dynamics of Ru^{II} (TPP)(CO), the lifetimes of $^1Q_{x(1,0)}(\pi,\pi^*)$ and $^1Q_{x(0,0)}(\pi,\pi^*)$ were determined to be (230±70) fs and (1 150±260) fs, respectively. Moreover, observed dynamic changes in the vibrational spectrum of υ_{por} from 1 040 to 1 150 cm^{-1} were identified to be changed in the spin state from the excited singlet state to the triplet state during the transition from the Franck-Condon state to the curve crossing point between the singlet and triplet. The decay time of the intersystem crossing including vibrational relaxation was determined to be (1.2±0.2) ps.

5　Acknowledgment

This work was supported by the grant from the Ministers of Education in Taiwan of China under the ATU Program at the National Chiao-Tung

University to A. Y. and T. K, and the 21st Century COE program on "Coherent Optical Science" to T. K.. The authors are grateful to the Information Technology Center of the University of Electro-Communications and the Information Technology Center of the University of Tokyo for their support of the DFT calculations.

6 Supporting Information

Calculation results are available free of charge via the Internet at http://pubs.acs.org.

References:

[1] BROWN G M, HOPF F R, FERGUSON J A, *et al*.. Metalloporphyrin redox chemistry. Effect of extraplanar ligands on the site of oxidation in ruthenium porphyrins[J]. *J. Am. Chem. Soc.*, 1973, 95(18):5939-5942.

[2] (a) RILLEMA D P, NAGLE J K, BARRINGER L F, *et al*.. Redox properties of metalloporphyrin excited states, lifetimes, and related properties of a series of para-substituted tetraphenylporphine carbonyl complexes of ruthenium(II)[J]. *J. Am. Chem. Soc.*, 1981,103(1):56-62.

(b) LEVINE L M A, HOLTEN D. Axial-ligand control of the photophysical behavior of ruthenium (II) tetraphenyl- and octaethylporphyrin: contrasting properties of metalloporphyrin (. pi.,. pi. *) and (d,. pi. *) excited states[J]. *J. Phys Chem.*, 1988,92(3):714-720.

(c) ANTIPAS A, BUCHLER J W, GOUTERMAN M, *et al*.. Porphyrins. 36. Synthesis and optical and electronic properties of some ruthenium and osmium octaethylporphyrins[J]. *J. Am. Chem. Soc.*, 1978,100(10):3015-3027.

[3] (a) PRODI A, INDELLI M T, KLEVERLAAN C J, *et al*.. Side-to-face ruthenium porphyrin arrays: Photophysical behavior of dimeric and pentameric systems[J]. *Chem. Eur. J.*, 1999,5(9):2668-2679.

(b) PRODI A, CHIORBOLI C, SCANDOLA F, *et al*.. Wavelength-Dependent Electron and Energy Transfer Pathways in a Side-to-Face Ruthenium Porphyrin/Perylene Bisimide Assembly[J]. *J. Am. Chem. Soc.*, 2005,127(5):1454-1462.

[4] (a) DANOVICH D, SHAIK S. Spin-Orbit Coupling in the Oxidative Activation of H－H by FeO^+. Selection Rules and Reactivity Effects[J]. *J. Am. Chem. Soc.*, 1997, 119:1773-1786.

(b) WANG Y, YANG C, WANG H, *et al*.. A new mechanism for ethanol oxidation mediated by cytochrome P450 2E1: Bluk polarity of the active site makes a difference[J]. *Chem. Bio. Chem.*, 2007, 8(3):277-281.

(c) MALTEMPO M M. Magnetic state of an unusual bacterial heme protein[J]. *J. Chem. Phys.*, 1974, 61:2540-2547.

(d) OHGO Y, IKEUEk T, TAKAHASHI M, *et al*.. Anomalous difference in magnetic behavior between highly saddled Iron(III) Porphyrin Complexes in the solid state[J]. *Eur. J. Inorg. Chem.*, 2004,2004(4):798-809.

[5] IWAKURA I, YABUSHITA A, KOBAYASHI T. Ultrafast vibronic processes in a Ru - Porphyrin complex[J]. *Eur. J. Inorg. Chem.*, 2008,2008(31):4856-4860.

[6] (a) KOBAYASHI T, SHIRAKAWA A. Tunable visible and near-infrared pulse generator in a 5 fs regime[J]. *Appl. Phys. B*, 2000,70(7):S239-S246.

(b) BALTUSKA A, FUJI T, KOBAYASHI T. Visible pulse compression to 4 fs by optical parametric amplification and programmable dispersion control[J]. *Opt. Lett.*, 2002,27(5):306-308.

[7] (a) KADISH K M, CHANG D. Solvent-binding and solvation effects on the electrode reactions of tetraphenylporphyrin carbonyl complexes of ruthenium(II)[J]. *Inorg. Chem.*, 1982,21(10):3614-3618.

(b) KADISH K M, LEGGETT D J, CHANG D. Investigation of the electrochemical reactivity and axial ligand binding reactions of tetraphenylporphyrin carbonyl complexes of ruthenium(II)[J]. *In-*

org. Chem. 1982,21(10):3618-3622.

[8] SAMOC A. Dispersion of refractive properties of solvents: Chloroform, toluene, benzene, and carbon disulfide in ultraviolet, visible, and near-infrared[J]. *J. Appl. Phys.* 2003,94(9):6167-6174.

[9] SORGUES S, POISSON L, RAFFAEL K, KRIM L, *et al*.. Femtosecond electronic relaxation of excited metalloporphyrins in the gas phase[J]. *J. Chem. Phys.* 2006,124:114302.

[10] The stimulated emission spectrum was calculated from the spontaneous emission spectrum of the sample excited at $\lambda_{exc}=515$ nm ($Q_x(1,0)$ band) and at $\lambda_{exc}=550$ nm ($Q_x(0,0)$ band), which were recorded on a HITACHI model F-4500 fluorescence spectrophotometer, using the relation between the Einstein coefficients A_{nm} (spontaneous emission) and B_{nm} (stimulated emission) given by $A_{nm}=(2hc/\lambda^3)B_{nm}$.

[11] The fluorescence spectra ($\lambda_{max}=560$ nm) of Ru^{II}(TPP)(CO)(dansyl-imidazole)
(a) LIM M H, LIPPARD S J. Inorg. Chem. 2004, 43, 6366-6370. That ($\lambda_{max}=556$ nm) of Ru^{II}(OEP)(CO)(py) (b) Hopf. F. R., O'Brien. T. P., Scheidt. W. R., Whitten. D. G. Structure and reactivity of ruthenium(II) porphyrin complexes. Photochemical ligand ejection and formation of ruthenium porphyrin dimmers[J]. *J. Am. Chem. Soc.*, 1975,97(2):277-281.

[12] (a) FUNATSU K, KIMURA A, IMAMURA T, *et al*.. Perpendicularly arranged ruthenium porphyrin dimers and trimers[J]. *Inorg. Chem.*, 1997,36(8):1625-1635.
(b) BHASIKUTTAN A C, SUZUKI M, NAKASHIMA S, *et al*.. Ultrafast fluorescence detection in tris(2,2'-bipyridine)ruthenium(II) complex in solution: relaxation dynamics involving higher excited states[J]. *J. Am. Chem. Soc.*, 2002, 124(28):8398-8405.

[13] Geometry optimizations were performed with B3LYP/6-31G* for model RuII(CO)(por).
(a) Frisch, M. J. Gaussian 03, revision, D. 02; Gaussian, Inc.: Wallingford, CT, 2004. Details are shown in the Supporting Information.
(b) Becke. A. D. Density - functional thermochemistry. III. The role of exact exchange[J]. *J. Chem. Phys.*, 1993,98:5648-5652.
(c) LEE C, YANG W, PARR R G. Development of the Colle-Salvetti correlation-energy formula into a functional of the electron density[J]. *Phys. ReV. B*, 1988, 37(2): 785-789.

[14] The metal-complex structure change during the chemical reaction causes the intersystem crossing.
(a) KHAVRUTSKII I V, MUSAEV D G, MOROKUMA K. Structure, Stability, and Electronic and NMR Properties of Various Oxo- and Nitrido-Derivatives of $[L(Salen)Mn(III)]^+$, Where L = None and Imidazole. A Density Functional Study[J]. *Inorg. Chem.*, 2003,42(8):2606-2621.
(b) IWAKURA I, IKENO T, YAMADA T. A DFT study on Hetero-Diels-Alder reactions catalyzed by cobalt complexes: lewis acidity enhancement as a consequence of spin transition caused by lewis base coordination[J]. *Angew. Chem. Int. Ed.*, 2005,44(17):2524-2527.
See also, Ref. 4(a) and (b).

[15] The heavy-atom effect is reported not to be a critical parameter in intersystem crossing of ^{1}MLCT $\rightarrow{}^3$MLCT of $M(bpy)_3$ complex in ref. (a-d). On the other hand, the heavy-atom effect was observed in intersystem crossing of $^1(\pi,\pi^*)\rightarrow{}^3(\pi,\pi^*)$ of M protoporphyrin in ref. (e). The existence of the heavy atomic effect is not sure in the present work of $^1(\pi,\pi^*)\rightarrow 3(d,\pi^*)$. Therefore, just a possibility of the heavy atomic effect was mentioned in the manuscript.
(a) CANNIZZO A, MOURIK F, GAWELDA W, *et al*.. Broadband Femtosecond Fluorescence Spectroscopy of $[Ru(bpy)_3]^{2+}$?[J]. *Angew. Chem. Int. Ed.*, 2006,45(19):3174-3176.
(b) GAWELDA W, CANNIZZO A, PHAM V T, *et al*.. Ultrafast nonadiabatic dynamics of $[Fe^{II}(bpy)_3]^{2+}$ in solution[J]. *J. Am. Chem. Soc.*, 2007,129(26):8199-8206.
(c) CANNIZZO A, BLANCO-RODRIGUEZ A M, NAHHAS A E, *et al*.. Femtosecond Fluorescence and Intersystem Crossing in Rhenium(I)

Carbonyl? Bipyridine Complexes [J]. *J. Am. Chem. Soc.*, 2008,130(28):8967-8974.

(d) BRESSLER C, MILNE C, PHAM V T, *et al*.. Femtosecond XANES Study of the Light-Induced Spin Crossover Dynamics in an Iron(II) Complex[J]. *Science*, 2009,323:489-492.

(e) KOBAYASHI T, STRAUB K D, RENTZEPIS P M. Energy relaxation mechanism in Ni(II), Pd(II), Pt(II) and Zn(II) porphyrins[J]. *Photochem. Phhotobiol.*, 1979,29(5):925-931.

Author's biography:

Takayoshi Kobayashi (1944—), male, was born in Niigata Prefecture, Japan, graduated from the University of Tokyo and got the bachelor, master, and doctor degrees from the same university. His major research directions are development of ultrashort pulse lasers, ultrafast spectroscopy of molecules, polymers, biomolecules, biopolymers, superconductors, strongly correlated materials, and semiconductors and laser microscopy. E-mail: kobayashi@ils.uec.ac.jp

●下期预告

折/衍混合自由曲面式头戴显示器光学系统设计

姜　洋[1,2],孙　强[1],谷立山[1],刘　英[1],李　淳[1],王　健[1]

(1.中国科学院 长春光学精密机械与物理研究所,吉林 长春 130033;
2.中国科学院 研究生院,北京 130039)

为解决传统头戴式显示器大视场、大出瞳距与小型轻量化之间的矛盾,设计了折/衍混合自由曲面式头戴显示器的光学系统。方法:利用衍射元件的特殊色散特性对系统进行色差校正;选取最佳的自由曲面面型组合对系统的像散、彗差、畸变进行校正;由光学塑料(PMMA)注塑成型的自由曲面棱镜形成离轴结构,使光学系统结构紧凑、便于装调。系统出瞳距离 17.4 mm,出瞳直径 4 mm,对角线视场,光学系统的点斑 RMS 直径小于,各视场光学调制传递函数在 30 lp/mm 时大于 0.1,系统畸变小于 10%。实际分析结果表明系统具有良好的成像质量,系统像差特性满足目镜系统的成像要求,可以达到虚拟现实各领域的实际需求。